The Offshore Structure and Subsurface Expression of Sea Level Variations off Peru, 1976–1977

ADRIANA HUYER

School of Oceanography, Oregon State University, Corvallis 97331

(Manuscript received 20 February 1980, in final form 15 July 1980)

ABSTRACT

Between April 1976 and May 1977, more than 35 repeated hydrographic sections were made just south of Cabo Nazca, Peru at 15°S, and sea level was measured continuously by a tide gage at San Juan. The sea level data were filtered to remove diurnal and shorter variations, and adjusted for the inverted barometer effect. For each hydrographic section, the dynamic height of the sea surface was computed relative to 500 and 600 db. Changes in the dynamic height at the station nearest the coast agree well with changes in the coastal sea level. The dynamic height data are therefore a good representation of the height of the sea surface along the section, and are used to examine the offshore structure of sea level fluctuations. The amplitude of these fluctuations decreases rapidly with distance from shore, with an offshore length scale of 30–60 km. The variations in sea level are associated with changes in the depth of subthermocline isotherms at depths of ~300–500 m, rather than with a change in the depth of the thermocline which remains between 50 and 100 m. The variations in sea level are also associated with fluctuations in the alongshore geostrophic velocity. Near the continental slope the amplitude of the geostrophic velocity fluctuations is constant down to ~300 m and then decreases rapidly down to ~500 m. These characteristics are consistent with the idea that the sea level variations are a manifestation of a poleward propagating internal Kelvin wave, with the interface at ~400 m rather than at the thermocline. Mean geostrophic velocity profiles show a poleward undercurrent with maximum southeastward flow of about 15 cm s^{-1} at a depth of 100 m near the continental slope (35 km from shore); the mean undercurrent is barely discernible 60 km from shore, and not observed 100 km from shore.

1. Introduction

Along the coast of central Peru, low-frequency (subtidal) fluctuations in sea level are not very well correlated with the local wind; instead, they propagate generally southward, apparently from an equatorial or near-equatorial source. Fluctuations with periods of days to weeks seem to be associated with baroclinic current fluctuations (Brink *et al.*, 1978) which have a poleward propagation speed of ~200 cm s^{-1}, consistent with an internal Kelvin wave propagating along the coast (Smith, 1978). Positive sea level anomalies that persist for several months or longer are associated with the El Niño phenomenon (Wyrtki, 1975); these also appear to propagate southward (Enfield and Allen, 1980), perhaps also as internal Kelvin waves (McCreary, 1976; Hurlburt *et al.*, 1976). In this paper, repeated hydrographic observations from a single section are used to demonstrate that the dynamic height of the sea surface computed from the hydrographic data agrees well with the coastal sea level data, to determine the offshore structure of the sea level variations, and to examine their subsurface expression in the temperature and geostrophic velocity fields.

2. The observations

An intensive field program called JOINT-II was conducted off Peru from March 1976 to May 1977 by the Coastal Upwelling Ecosystems Analysis (CUEA) program. The observations were concentrated in the region just south of Cabo Nazca and included repeated occupations of a central hydrographic section (the "C-line") extending approximately southwestward from the coast (Fig. 1). Thirty-seven sections were concentrated in three periods: 27 April–23 June 1976, 27 July–14 August 1976 and 5 March–16 May 1977 (Fig. 2). Almost all of these sections included CTD casts at each station, down to 500 m or deeper at the offshore stations; the CTD sampled at depth intervals of a few meters or less. During a few of the sections, the CTD system was inoperable and Niskin bottle casts were made instead.

Observations during the first period (27 April–23 June 1976) were made from the R.V. *T. G. Thompson* with a Plessey 9040 CTD system (Barton, 1977; Friebertshauser *et al.*, 1977). During this period the central hydrographic section was directed toward 240°T (Fig. 1), and the most inshore station was ~2–3 km from shore. During the second period (27

0022-3670/80/111755-14$07.50

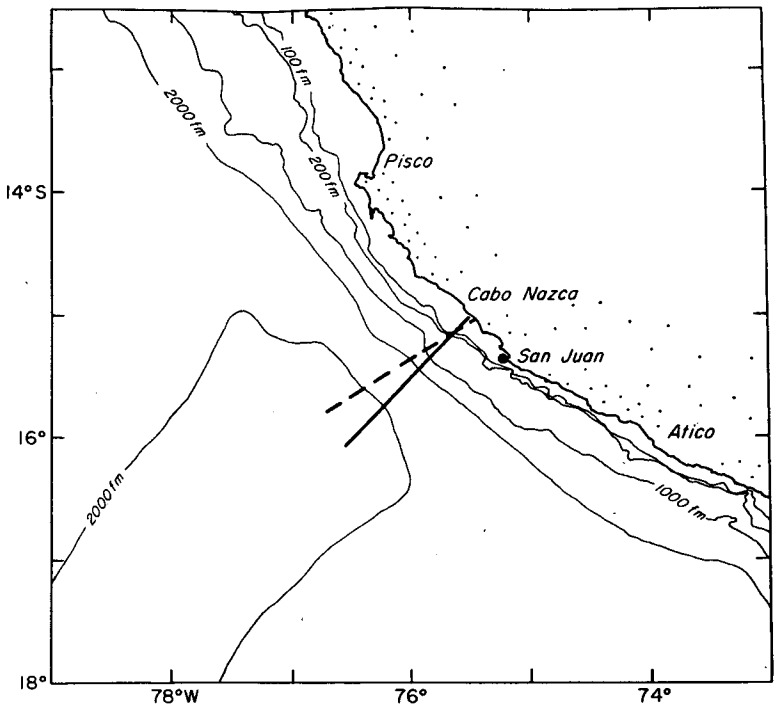

FIG. 1. Location of the JOINT-II central hydrographic section (the "C-line") and the tide gage at San Juan. The dashed line shows the C-line occupied by the *Thompson*, and the solid line shows that occupied by the *Eastward, Melville* and *Iselin*.

July–14 August 1976) the observations were made from the R.V. *Eastward* with a Geodyne CTD system (Huyer *et al.*, 1978a); the orientation of the section was changed to 225°T to be more nearly perpendicular to the coastline, and the inshore station was 4–6 km from the coast. During the third period (5 March–16 May 1977) observations were made alternately from the R.V. *Melville* and the R.V. *C. O'D. Iselin* with the Geodyne CTD system (Huyer *et al.*, 1978b); the orientation of the section was still toward 225°T, and the most inshore station was 2–3 km from the coast. During all three periods the stations were about 3 n mi (5.5 km) apart over the shelf and upper continental slope, 6 n mi (11 km) apart out to about 70 km from the coast, and about 12 n mi (22 km) apart farther offshore. The Geodyne and Plessey CTD systems have similar resolution in temperature, depth and conductivity and similar *in situ* calibration procedures were used with both.

Sea level is measured routinely at San Juan and hourly data are available; for the period of the JOINT-II study we also had access to the original tide gage records, and some small corrections (all < 5 cm) were incorporated in the hourly time series. The hourly data were filtered to eliminate diurnal and higher frequencies by means of a symmetrical low-pass filter spanning 121 h. The filter passes signals with 0.5% amplitude at 1 cpd (cycles per day), 50% amplitude at 0.7 cpd, 71% amplitude (half-power) at 0.6 cpd, and 95% amplitude at 0.5 cpd. The resulting series were decimated to six-hourly values. Daily average atmospheric pressure data were available from an airport several kilometers from the tide gage. The daily values were interpolated to provide six-hourly data which were used to "adjust" the sea level for the "inverted barometer effect," which assumes that a pressure increase of 1 mb decreases sea level by 1 cm. The low-passed adjusted sea level (Fig. 2) was generally high during the first period of repeated hydrographic sections and highly variable during the second; sea level was generally low during most of the third period.

3. Dynamic height as a measure of sea level

The contribution of density variations to changes in the height of the sea surface can be determined from the density profile if the ocean is assumed to be in hydrostatic balance, i.e.,

$$g dz = \alpha dp,$$

where g is the acceleration due to gravity, α the specific volume, and dz and dp are small increments in depth and pressure. Integrating over depth, and

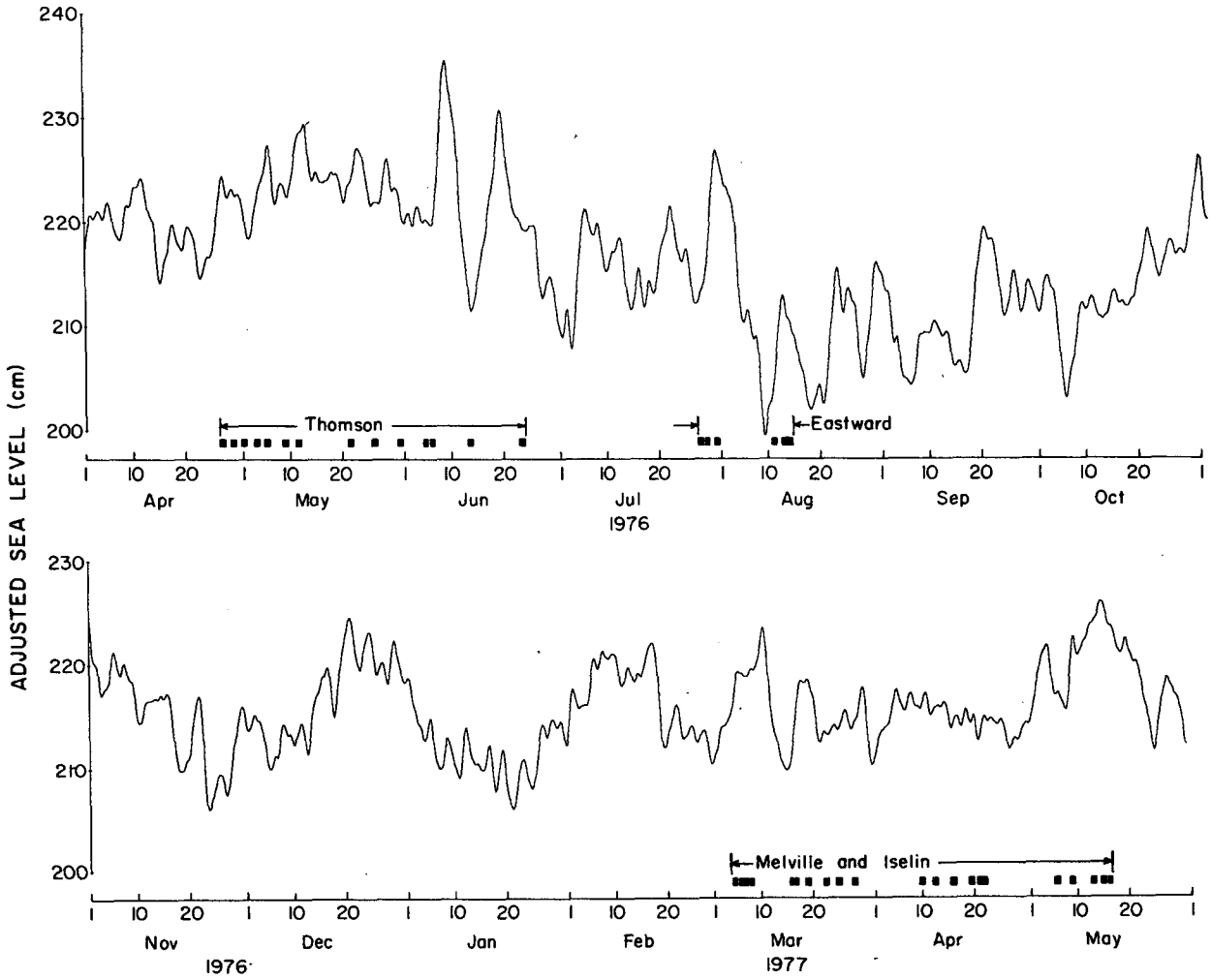

FIG. 2. The time series of low-pass filtered adjusted sea level at San Juan, April 1976–May 1977. CTD sections along the C-line are indicated by square dots.

converting to common oceanographic units (depth in m, pressure in db, specific volume in $cm^3\ g^{-1}$ and acceleration in $m\ s^{-2}$), we obtain the vertical separation between any two isobars:

$$z = 10\int_{p_1}^{p_2}\frac{\alpha}{g}dp \approx \frac{10}{g}\int_{p_1}^{p_2}\alpha dp$$
$$= \frac{10}{g}\int_{p_1}^{p_2}\alpha_{35,0,p}dp + \frac{10}{g}\int_{p_1}^{p_2}\delta dp,$$

where $\alpha_{35,0,p}$ is the specific volume of sea water at 0°C and 35‰ and δ is the specific volume anomaly. The first of the two terms on the right is constant, so variations in the separation z' depend only on the second term. The integral in the second term generally is called the geopotential anomaly or dynamic height anomaly ($\Delta D_{p_1/p_2}$); it is routinely computed from hydrographic data and has units of dynamic meters (dyn m). Thus,

$$z' = \frac{10}{g}\Delta D_{p_1/p_2},$$

i.e., changes in the separation between isobars are directly proportional to changes in dynamic height, and the constant of proportionality is very close to 1. If the upper isobar is the sea surface ($p_1 = 0$ db) and the lower isobar remains at a constant depth, variations in $\Delta D_{0/p_2}$ represent changes in the sea level due to density variations.

Additional computations are required to obtain the dynamic height near the coast if the bottom there is shallower than the reference level (isobar p_2). Near Cabo Nazca, the 500 and 600 db surfaces intersect the bottom ~30 km from shore. To obtain the dynamic height nearer shore, geopotential surfaces were extrapolated toward the coast by the method described by Reid and Mantyla (1976). This method requires at least two offshore stations down to

TABLE 1. The repeated sections along the "C-line," the dynamic height at the most inshore station, and the simultaneous sea level at the San Juan tide gage.

Date	Section		Inshore station					Tide gage	
	Stations	Length (km)	Station	Distance from shore (km)	Day/Time (GMT)	ΔD 0/600	ΔD 0/500	Day/Time (GMT)	Sea level (cm)
Thompson, 1976									
26–27 Apr	1–12	92	12	2.2	27/1445		87.5	27/1200	224.0
28–29 Apr	13–21	60	13	3.5	28/1135		88.7	28/1200	222.5
30 Apr–1 May	38–46a	60	38	2.8	30/2318	95.9	84.5	1/0000	221.8
3 May	82–88	38	82	2.0	3/1545		84.8	3/1000	222.0
5 May	89–97	60	97	2.4	5/0110		88.3	5/0000	224.4
8–9 May	106–120	190	120	1.8	8/0600	100.7	88.8	8/0600	223.6
11 May	121–127a	37	121	2.0	11/0202		86.1	11/0600	227.2
21 May	128–134	38	128	1.8	21/0133	97.0	87.0	21/0600	223.6
25–26 May	136–143	48	136	1.8	25/2333		86.7	26/0000	221.7
30–31 May	144–151	49	144	2.0	30/2312		91.0	31/0000	222.7
4–6 Jun	161–172	69	161	3.1	4/2213	98.6	89.1	5/0000	220.2
13 Jun	185–196	50	185	2.0	13/0820		78.6	13/1200	212.0
23 Jun	291–297	50	291	1.3	23/1548	103.8	91.0	23/1800	219.2
Eastward, 1976									
27–28 Jul	12–16	42	12	5.6	27/1905	94.8	84.2	28/0000	213.3
28–29 Jul	17–29*	187	17	3.9	28/1622		91.8	28/1800	214.2
30–31 Jul	30–40	116	30	3.9	30/1517	110.0	97.8	30/1800	226.4
10–11 Aug	69–86	111	86	5.6	11/0120	80.7	71.8	11/0000	203.8
12–14 Aug	98–118	200	118	6.5	14/0327	84.9	76.4	14/0000	210.5
Melville and *Iselin*, 1977									
4–5 Mar	3–12	42	3	2.4	4/2130	92.6	82.0	5/0000	217.1
5–6 Mar	13–23†	24	13	2.6	5/2220			6/0000	219.1
6–8 Mar	24–36	141	24	7.4	6/2140		86.9	7/0000	218.8
15–16 Mar	48–55	40	48	1.8	15/2250	95.4	86.1	16/0000	211.1
16 Mar	57–61†	25	61	1.5	16/2132			17/0000	216.0
18–19 Mar	77–93	183	93	1.5	19/2137	93.7	82.9	20/0000	217.0
22 Mar	119–125	36	125	2.8	22/1251	86.0	74.5	22/1200	213.4
24–25 Mar	154–160	33	154	1.5	24/2222	94.8	84.2	25/0000	213.5
27–28 Mar	162–181	166	162	2.6	27/1245	91.7	81.9	27/1200	213.6
9–10 Apr	204–215	143	204	1.1	9/1204	89.7	79.4	9/1200	215.7
12 Apr	227–235	55	235	2.0	12/0139	89.4	79.4	12/0000	215.1
15–16 Apr	257–271	164	271	1.8	15/1330	91.8	81.4	15/1200	214.0
19 Apr	321–328‡	46	328	1.8	19/2221			20/0000	215.0
20–22 Apr	344–358	164	344	2.2	20/2119	83.1	72.9	21/0000	212.5
5–6 May	363–376*	164	363	5.4	5/0132	95.5	83.3	5/0000	218.5
8–9 May	382–391	73	391	2.4	9/2001	92.8	81.8	9/1800	220.7
12–13 May	409–417*	98	409	1.5	12/2005	99.9	87.1	12/1800	223.7
14–15 May	802–810	36	802	3.1	14/1002	99.2	86.8	14/1200	225.8
15–16 May	424–432	62	432	1.8	16/0918		89.2	16/1200	223.3

* CTD data not available at all stations.
† Only one station down to 500 db.
‡ No stations down to 500 db.

the reference level: the dynamic height at the maximum pressure of the next inshore station is computed by linear extrapolation from the values of the dynamic height at this pressure at the two offshore stations; it is then possible to compute the dynamic height relative to the chosen reference level for the entire column at the inshore station, and the extrapolation process can be repeated to the most inshore station. During JOINT-II, the most inshore station was only a few kilometers from the coast, and therefore the dynamic height at the inshore station (Table 1) is probably a good estimate of the dynamic height at the coast.

Comparison of the $\Delta D_{0/500}$ and $\Delta D_{0/600}$ at the most inshore station with the simultaneous low-passed adjusted sea level at San Juan (Fig. 3) shows good correlation. If all pairs are independent, the correlation coefficients (r) are significantly different from zero at the 99.9% level (Pearson and Hartley, 1970, p. 146). If only half the pairs were independent, that is, if the number of degrees of freedom was 15 for the $\Delta D_{0/500}$ and 9 for the $\Delta D_{0/600}$ comparison

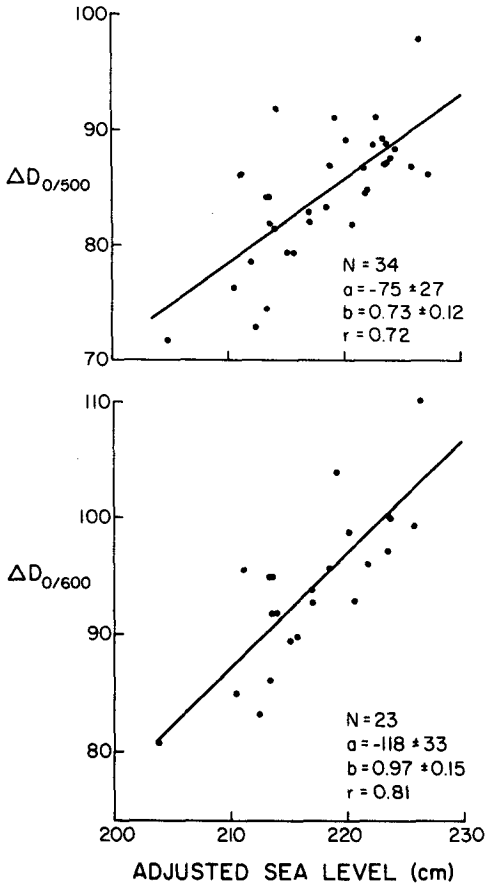

FIG. 3. The dynamic height of the sea surface at the inshore station of each section, relative to the 500 and 600 db pressure surfaces, plotted as a function of the simultaneous value of adjusted sea level at San Juan. The number of points (N), the correlation coefficient (r) and the intercept (a) and slope (b) of the regression line are shown for each comparison.

with sea level, the significance level would be 99.5%. Even if only a third of the pairs were independent (there were 9 and 6 degrees of freedom, respectively), the correlations would still be significantly different from zero at the 98% level. The autocorrelation function of adjusted sea level suggests that data points more than 8 days apart are independent, and Fig. 2 visually supports this estimate. Thus it seems likely that at least a third of the points in Fig. 3 are independent, and the correlations are significant at least at the 98% level.

Linear regression of dynamic height on sea level yields a regression coefficient (b) significantly less than 1 for $\Delta D_{0/500}$—i.e., changes in density above 500 m do not completely account for the observed variation in sea level. The regression coefficient between $\Delta D_{0/600}$ and sea level is essentially equal to 1, and $\Delta D_{0/600}$ accounts for 66% of the variance in sea level. The range of these two variables is also similar (29.3 dyn cm for $\Delta D_{0/600}$ and 23.6 dyn cm for the simultaneous values of sea level) and all of the points lie within 6 cm of the regression line. The errors associated with the shoreward extrapolation of dynamic height relative to the 600 db surface can certainly account for the discrepancies. Thus, the density changes above 600 m account almost entirely for the observed changes in sea level.

Good agreement between the dynamic height of the sea surface relative to 500 or 600 db and sea level is generally expected for long time scales (a month or more) and long space scales (100 km or more). Our results show good agreement even with relatively short length scales in a coastal region—many of our sections were shorter than 50 km (Table 1). The excellent agreement between $\Delta D_{0/600}$ and the simultaneous adjusted sea level

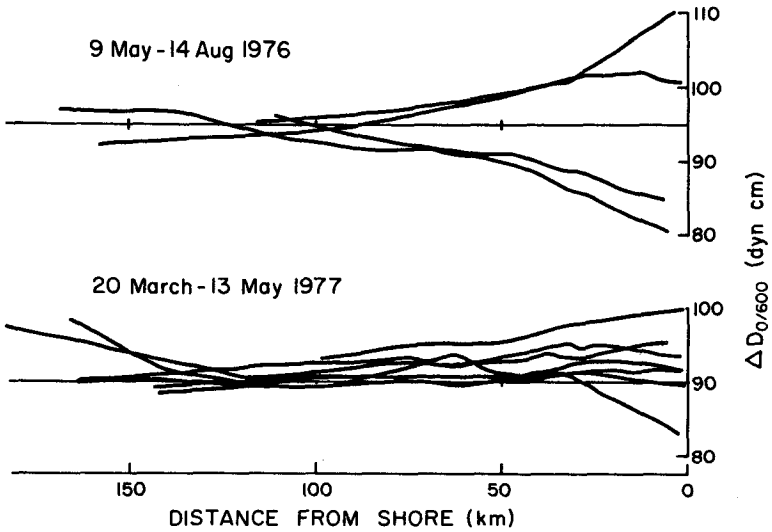

FIG. 4. The offshore profiles of dynamic height of the sea surface relative to 600 db, for all sections longer than 90 km.

indicates that the baroclinic adjustment process occurs very quickly, and that the short-term fluctuations in sea level are very quickly reflected in the density field or vice versa; a similar result has been obtained off Baja California (Christensen and Rodríguez S., 1979).

4. Offshore profiles of the sea surface

The good agreement between the dynamic height and sea level at the coast implies that $\Delta D_{0/600}$ is a good estimator of sea level offshore as well as at the coast. Eleven of the repeated sections extended 100 km or more offshore as well as down to 600 db (Table 1). The offshore profiles of $\Delta D_{0/600}$ from these sections (Fig. 4) show that the largest sea level variations occurred near shore, and that sea level was much less variable 90–140 km from shore.

The offshore sea level seems to be somewhat higher during the 1976 sections than during the 1977 sections. The mean value of $\Delta D_{0/600}$ at 100 km from shore is about 94 dyn cm for the four sections between 9 May and 14 August 1976, and about 91 dyn cm for the seven sections between 20 March and 13 May 1977. This change is very small and may not be significant; its sign is opposite to what one would expect from the influence of the seasonal heating and cooling cycle.

The large variations in sea level seem to be trapped near the coast: the range decreases monotonically from the coast to about 80 km from shore (Fig. 4). Although we do not know the mean offshore profile of sea level, we may assume as a first approximation that it is level, i.e., that the mean sea level is the same near shore as it is at 100 km from shore. The observed profiles may then be considered as deviations from this level surface. In the profiles with the largest coastal elevations, the amplitude of the deviation decreases monotonically with distance from the coast. In the two extreme profiles (observed on 30 July and 11 August 1976), the coastal sea level differs about 15 cm from the constant offshore value at 100 km and the amplitude decays very nearly exponentially with distance from shore. Regressing the natural logarithm of the sea level deviation for these dates on distance from shore yields length scales of 31 and 37 km, with correlation coefficients of 0.98 and 0.99, respectively. In four additional profiles, the coastal sea level differed from the offshore sea level by 5–10 cm; although these profiles were not strictly exponential, their offshore length scales were also estimated by regressing the natural logarithm of the sea level deviation on distance from shore, and found to be 27, 48, 50 and 59 km.

For comparison with these observed length scales, we computed the Rossby radius of deformation from the stratification observed offshore. The radius of deformation is the radius of an inertial circle corresponding to the velocity of long waves in a flat-bottomed ocean (Rossby, 1938). We used the profiles of Brunt-Väisälä frequency (N) at stations 100 km from shore, extrapolated exponentially from the deepest observation at ~800 m to $N = 0.115$ cph at the bottom at 4000 m, to compute the phase speed of the first-mode long wave (Kundu *et al.*, 1975, Section 5). The values of phase speed c ranged from 180 to 290 cm s^{-1}. These calculated phase speeds agree well with the propagation of sea level fluctuations along the Peru coast (Smith, 1978). Values of the Rossby radius of deformation λ computed from these phase speeds ($\lambda = c/f$, where f is the Coriolis parameters) range from 48 to 77 km.

The offshore length scales (27–59 km) estimated from the offshore profiles of dynamic height are quite similar to the estimates of the Rossby radius (48–77 km), although they tend to be smaller. Both are similar to the width of the continental shelf and slope—the distance from the coast to the 1000 fathom contour is ~55 km (Fig. 1).

5. Subsurface temperature variability

The largest change in sea level during the 14-month JOINT-II observation period occurred in early August 1976, when sea level fell from a maximum of 227 cm on 31 July to a minimum of 201 cm on 9 August (Fig. 2). Four CTD sections were made at about this time (Table 1): on 27–28 July, before sea level rose to its maximum; on 30–31 July, during the maximum; on 10–11 August, just after the minimum; and on 12–14 August, several days after the minimum (Fig. 2). Between the sections of 30–31 July and 10–11 August, the sea level at San Juan decreased by 22.6 cm (Table 1). Between these dates, all isotherms between 6 and 16°C (at depths between ~100 and 600 m) rose by roughly 100 m along the continental margin (Fig. 5). The 7°C isotherm shows the largest change in depth (~180 m) while the 15°C isotherm shows the smallest change (~75 m). The isotherm displacements between these two dates decay rapidly with distance from shore (Fig. 5), to about 50 m at 50 km from shore, and to less than 20 m at 75 km from shore.

To determine whether the subsurface changes during this extreme event were typical, we examined subsurface isotherms for each of the repeated sections. Table 2 shows depths of selected isotherms at stations approximately over the mid-slope, i.e., where the water depth was about 800–1500 m. In general, the "mid-slope" station of each section is the station nearest shore that extended to the maximum depth of the section (usually 500 or 600 m). Since the continental slope rises rather steeply to the shelf break at about 150 m (Fig. 5), these isotherm depths are a good estimate of the depths of the

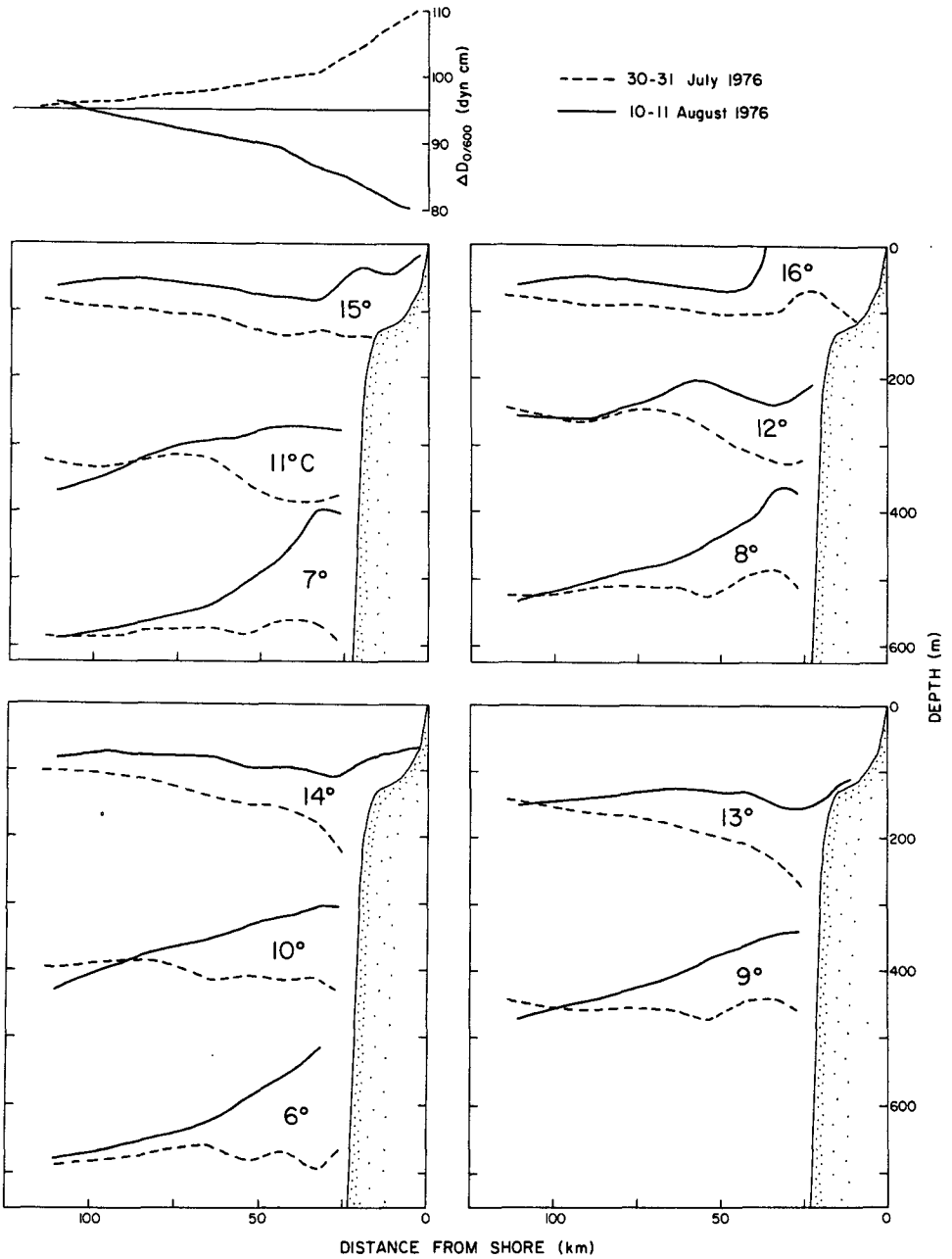

FIG. 5. Offshore profiles of $\Delta D_{0/600}$ (representing the sea surface) and of selected isotherms at times of very high and very low sea level (on 31 July and 10 August, respectively). Isotherms have been separated for clarity.

inshore end of the deeper isotherms. The depths of the 7, 9 and 11°C isotherms are significantly correlated with sea level and the regression lines have slopes of ~7 (Fig. 6). Thus, each of these isotherms descends by about 7 m when sea level increases by 1 cm. The 13°C isotherm is also correlated with sea level but the regression coefficient is smaller—the 13°C isotherm descends only 3.5 m when sea level increases 1 cm. The depth of the 14°C is only weakly correlated with sea level and the regression coefficient is again smaller: the 14°C isotherm descends only 2 m when sea level rises 1 cm. If all samples are independent, the correlation coefficients for the 7, 9, 11 and 13°C isotherms are all significantly different from zero at the 99.9% level, the correlation coefficient for the 14°C is significant at the 95% level, and the correlation coefficient for the 15°C isotherm is not significant

TABLE 2. Depth of selected isotherms at the "mid-slope" station of each section and the simultaneous adjusted sea level at San Juan, for the repeated hydrographic sections just south of Cabo Nazca.

Station	Distance from shore (km)	Date	Time (GMT)	Isotherm depths (m) 7°C	9°C	11°C	13°C	14°C	15°C	Sea level (cm)
Thompson, 1976										
7	28	27 Apr	0930	600	476	374	246	133	84	224.0
18	29	28 Apr	1833	558	490	396	221	126	66	222.9
43	29	1 May	0615	566	464	344	208	107	64	220.9
87	30	3 May	2045	>492	460	370	194	96	66	222.0
92	29	5 May	0700	568	482	408	225	123	52	223.3
115	28	9 May	0455	>600	522	396	220	152	110	223.0
126	29	11 May	0724	>596	558	420	210	141	98	227.2
133	30	21 May	0719	530	432	360	187	153	110	223.6
141	29	26 May	0510	>502	424	356	233	121	68	221.9
150*	38	31 May	0935	>498	472	326	158	143	120	220.8
166	28	5 Jun	0542	>500	468	386	221	147	116	220.3
194	29	13 Jun	1910	>500	448	336	169	122	76	211.4
295	28	23 Jun	1943	598	476	366	221	198	148	219.2
Eastward, 1976										
14	31	27 Jul	2217	549	445	320	196	146	122	212.7
34	28	30 Jul	1834	590	457	375	272	221	139	226.4
80	26	10 Aug	2049	408	340	280	158	110	64	202.9
112	30	13 Aug	1929	508	377	258	109	84	78	210.7
Melville and *Iselin*, 1977										
8	30	4 Mar	0216	>466	396	306	203	152	71	214.7
23†	24	6 Mar	0857	526	428	339	213	133	65	219.0
29†	24	7 Mar	0234	>494	406	330	248	126	55	218.8
53	30	16 Mar	0425	507	384	296	166	80	64	212.2
57†	25	16 Mar	1736	505	396	307	178	104	65	214.6
88	29	19 Mar	1339	534	400	312	194	123	88	217.9
120	31	22 Mar	0638	500	352	260	150	108	76	213.4
159	30	25 Mar	0320	524	372	283	190	114	68	213.8
167	32	27 Mar	1931	517	366	271	176	130	68	213.7
209	30	9 Apr	2144	522	372	286	168	156	114	215.8
230	30	12 Apr	0822	514	392	296	181	153	92	215.4
266	30	16 Apr	1313	512	401	328	185	118	82	214.8
323	29	19 Apr	1819	>324	>324	292	212	150	74	214.5
349	30	21 Apr	0447	550	363	282	187	151	79	213.0
386	30	9 May	0902	590	438	307	194	153	84	221.5
413*	36	13 May	0914	596	457	364	221	138	80	224.4
809	31	15 May	0022	608	470	370	205	130	74	225.5
428	29	16 May	0255	>568	459	348	194	139	84	223.5

* No CTD station over the mid-slope; station farther from shore.
† No CTD station over the mid slope; station nearer shore.

even at the 90% level (Pearson and Hartley, 1970). If only a third of the samples are independent, the correlation coefficients for the 7, 9 and 11°C isotherms are still significant at the 99.5% level, the correlation for the 13°C isotherm is significant at the 95% level, but the correlation for the 14°C is not significant even at the 90% level. Since the inshore ends of the 14 and 15°C isotherms were usually over the continental shelf, we repeated the comparison with sea level using the depth of the most inshore observation of these isotherms: the results were very nearly identical to those presented in Fig. 6.

Both the statistics for the entire JOINT-II period and the single event in August 1976 show the same behavior of subsurface isotherms. The deeper isotherms at depths between 300 and 600 m show the largest changes in depth, and the depths of these isotherms (7 and 9°C) have the highest correlation with sea level. Shallower isotherms show progressively smaller variations in depth and their depths are progressively less correlated with sea level.

Most previous studies relating variations in sea level along the Peruvian coast to the subsurface temperature variability have considered only changes in the depth of the thermocline. In the eastern tropical Pacific Ocean, the main thermocline is quite shallow, generally above 200 m (Tsuchiya, 1968, 1975). The temperature at the bottom of the thermocline is about 13°C; the temperature at the top of the

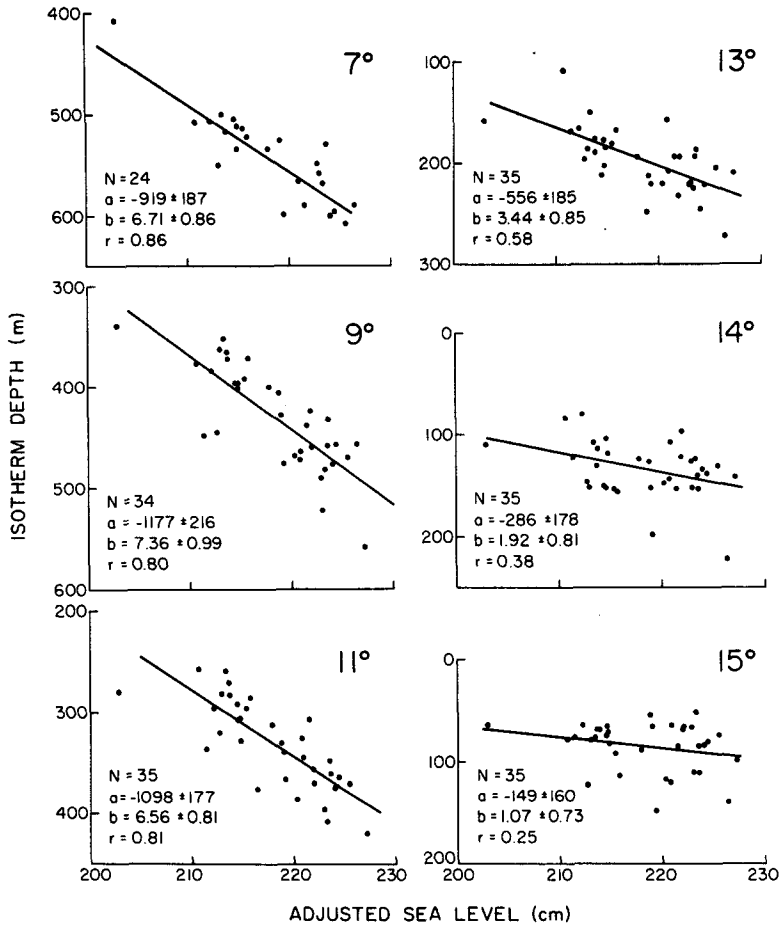

FIG. 6. Scatter diagrams and linear regression lines between isotherm depth and simultaneous adjusted sea level at San Juan, for selected isotherms at the mid-slope station of each section.

thermocline varies with season and location. Off Cabo Nazca, a well-defined thermocline is observed between 50 and 125 m at locations more than 50 km from the coast; the isotherms within the thermocline (13–15 or 16°C in winter and 13 to 18 or 20°C in summer) diverge as they approach the coast (Robles P. and Barton, 1977; Friederich *et al.*, 1977; Huyer and Gilbert, 1979). Thus isotherms warmer than 15°C slope generally upward toward the coast, while those cooler than 15°C slope generally downward toward the coast. The depth of the 15°C isotherm is therefore a reasonable estimator of the depth of the thermocline.

Wyrtki (1975) showed that the 15°C isotherm was much deeper near shore during the 1972 El Niño than during the normal periods in 1964 and 1967, by as much as 100 m off Callao and even more off northern Peru. Since sea level was well above normal during the 1972 El Niño and near normal in 1964 and 1967, Wyrtki (1975) implies a relationship between sea level and the depth of the 15°C isotherm or, in other words, between sea level and the depth of the thermocline. Several theoretical studies have modeled the sea level variations along the Peruvian coast as Kelvin waves in a two-layer fluid, with the interface between the two layers at about the depth of the thermocline. Hurlburt *et al.* (1976) used an upper layer thickness of 120 m with a density difference of 3×10^{-3} g cm^{-3}; McCreary (1976) used upper layer thickness of 100 and 200 m with a density difference of 4×10^{-3} g cm^{-3}; Allen and Romea (1980) used an upper layer thickness of 70 m with a density difference of 1.5×10^{-3} g cm^{-3} and an upper layer thickness of 100 m with a density difference of 2.5×10^{-3} g cm^{-3}. All of these models use an interface depth corresponding roughly to the depth of the main thermocline and the 15°C isotherm. The largest change in interface depth for a given change in sea level occurs in the model with the smallest density difference, i.e., in the models of Allen and Romea (1980).

Comparison between these two-layer models and

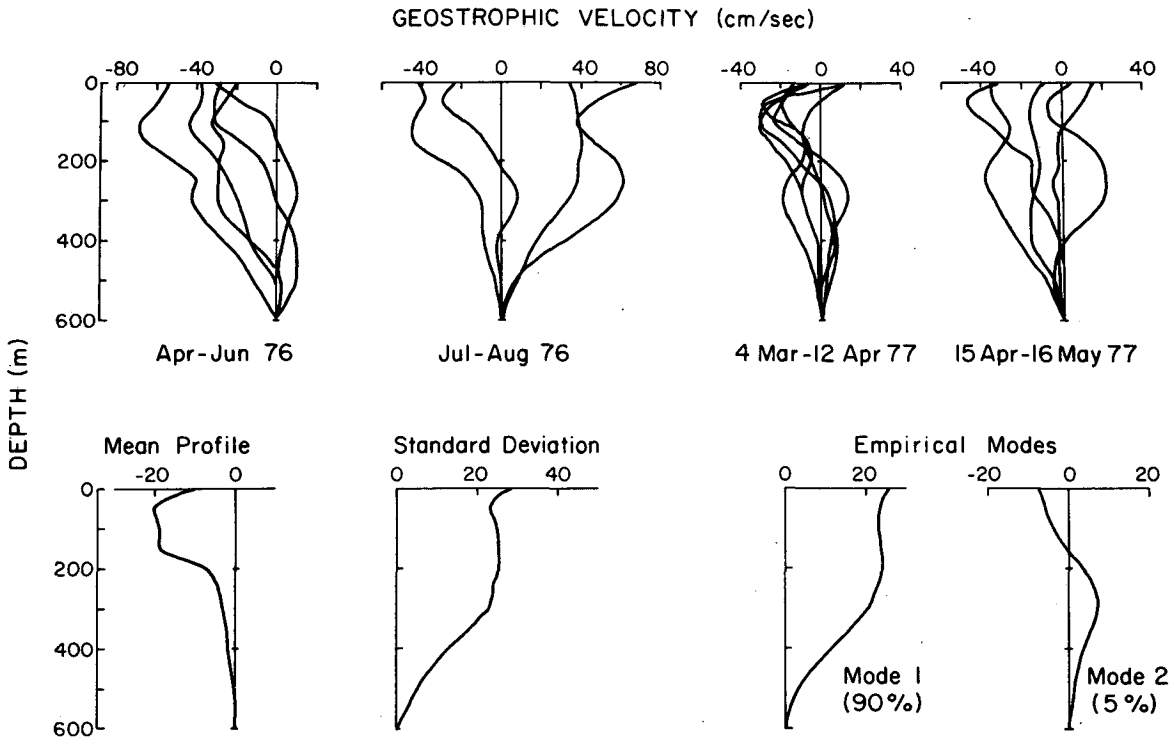

FIG. 7. Vertical profiles of the geostrophic velocity relative to 600 db at about 35 km from shore, just seaward of the continental slope. Positive velocities are northwestward (equatorward) and negative velocities are southeastward (poleward). Velocities were computed from 20 station pairs, separated by ~12 km. Shown are the individual profiles, the mean and standard deviation, and the first two empirical orthogonal modes computed from all 20 profiles.

our observations suggest that the choice of a density difference of 1.5×10^{-3} g cm^{-3} across the interface is reasonable, but that the choice of the depth of the upper layer is not. The regression coefficients between isotherm depth and sea level have values of ~7 m cm^{-1} for those isotherms which are strongly correlated with sea level (i.e., the 7–11°C); these agree very well with the ratio of 6.7 m cm^{-1} obtained from a two-layer model with a density difference of 1.5×10^{-3} g cm^{-3}. The vertical distributions of sigma-*t* (Robles P. and Barton, 1977; Friederich *et al.*, 1978; Huyer and Gilbert, 1979) also indicate that this density difference is appropriate for most of the JOINT-II sections off Cabo Nazca. Our observations indicate that the depth of the thermocline and the associated shallower (14 and 15°C) isotherms are not well correlated with sea level (Fig. 6). These isotherms are quite shallow, and their depths are probably affected by local processes (such as surface heating and cooling) as well as by the density fluctuations associated with changes in sea level. Variations in sea level are strongly associated with subthermocline isotherms at depths between 300 and 600 m, including the 7, 9 and 11°C isotherms. If these variations are to be modeled with a two-layer system, the interface should be at 400–500 m, considerably deeper than the thermocline. A model with continuous stratification is probably even more suitable.

Our results may not be applicable to distant locations along the coast of South America. For example, Enfield (1980) shows a very large change occurred between November–December 1971 and February–March 1972 in the depth of the 15°C isotherm off Ecuador while the 10°C isotherm remained at about the same depth. Apparently, the large changes in isotherm depth are restricted to the eastern boundary region. Meyers (1979) shows that the depth range of the 14°C isotherm along the equator is less than 100 m across the entire Pacific except east of 95°W, where the range increases to 200 m. This intensification along the eastern boundary is consistent with the generation of the fluctuations along the equator (McCreary, 1976; Hurlburt *et al.*, 1976).

6. Geostrophic velocity profiles

The vertical structure of the fluctuations can perhaps be most clearly seen in the profiles of geostrophic velocity. Geostrophic velocity calculations from closely spaced stations are subject to rather large uncertainties: small errors in the dynamic height data may lead to large errors in its hori-

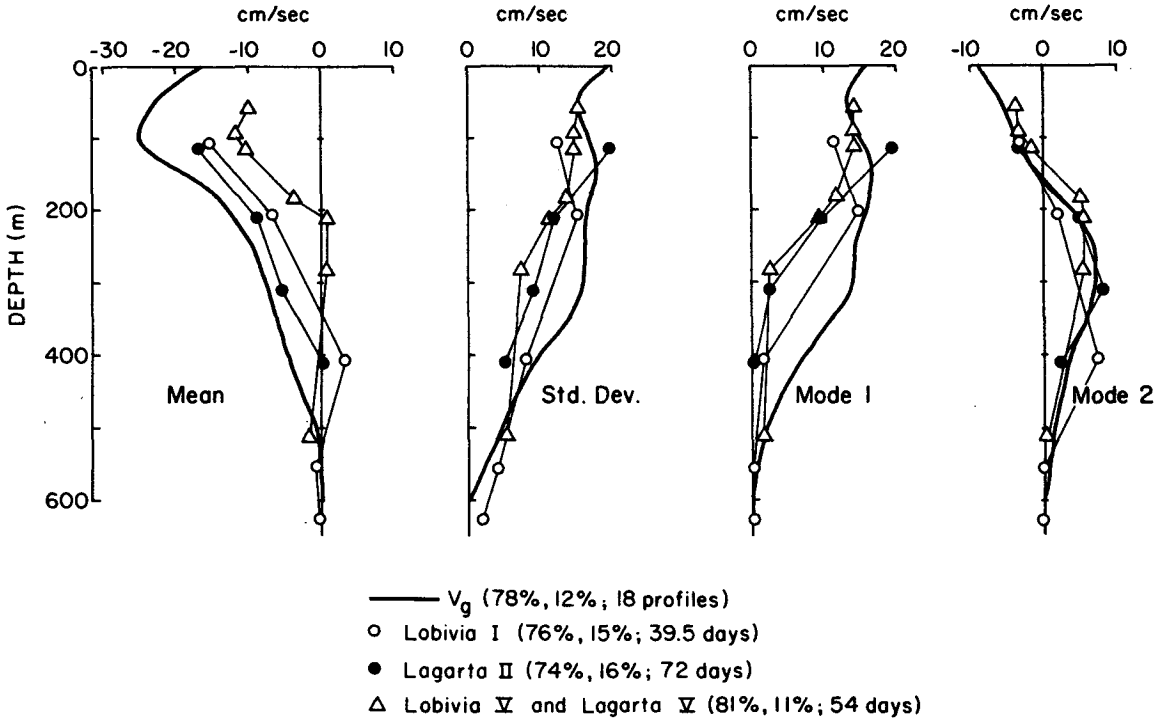

FIG. 8. The mean, standard deviation and first two empirical orthogonal modes of 18 profiles of near-slope geostrophic velocity (V_g) relative to 600 db, calculated from sections occupied during 1 May–31 July 1976 and 4 March–15 May 1977. Also shown are statistics for current meter moorings over the upper slope: *Lobivia* I, during 28 March–6 May 1976; *Lagarta* II, during 15 May–26 July 1976; *Lagarta* V and *Lobivia* V, during 22 March–10 May 1977.

zontal gradient. Navigation errors also contribute significant uncertainties—an error of ±1 km may cause errors as large as 20% if the station separation is 10 km. Nevertheless, we expect the structure of the profiles to be representative because these errors are independent of depth.

We computed geostrophic velocities relative to 600 db for a location just seaward of the continental slope. The location varied slightly from section to section, from 32 to 38 km from shore. We used only pairs of stations separated by at least 7.6 km and no more than 16.5 km; the separation was usually between 9 and 12 km. Twenty sections included station pairs that met these criteria, and for these we computed the geostrophic velocity at nine depths—at 50 m intervals down to 300 m and at 400 and 500 m (Fig. 7). Most of the profiles have a relative minimum between 50 and 150 m, which is seen most clearly in the mean profile, and which corresponds to the poleward undercurrent observed with current meters moored over the continental slope and shelf (Brink *et al.*, 1978, 1980). The profile of the standard deviation of the geostrophic current (Fig. 7) suggests that the amplitude of the fluctuations is uniform in the upper 300 m, and that it decreases rapidly between 300 and 500 m.

Empirical-orthogonal function analysis of the fluctuating part of the geostrophic velocity showed that 95% of the variance is accounted for by the first two modes. The first mode, which contains 90% of the variance, has nearly uniform amplitude down to 300 m, and large vertical shear between 300 and 500 m (Fig. 7). The large shear in the geostrophic velocity at this depth is consistent with the large variations in the depth of the 7, 9 and 11°C isotherms (Fig. 6). In spite of the errors in the geostrophic computations, the amplitude of the first empirical mode is significantly correlated with the adjusted sea level ($r = 0.77$, $N = 20$), at the 99.9% level if all samples are independent and at the 95% level if only a third of them are independent. Linear regression between the first mode and sea level indicates that the geostrophic velocity between the surface and 300 m increases 3.5 cm s^{-1} when sea level falls by 1 cm. The second empirical mode, which contains only 5% of the total variance, has a zero-crossing at 150 m and a maximum at 300 m (Fig. 7). This mode is not at all correlated with the adjusted sea level ($N = 20$, $r = 0.05$).

Current meter moorings were maintained over the continental slope during three periods within JOINT-II: *Lobivia* I, with five current meters, during 26 March–6 May 1976; *Lagarta* II, with four current meters, during 11 May–30 July 1976; and *Lobivia* V and *Lagarta* V, with a total of seven current meters, during 15 March–15 May 1977 (En-

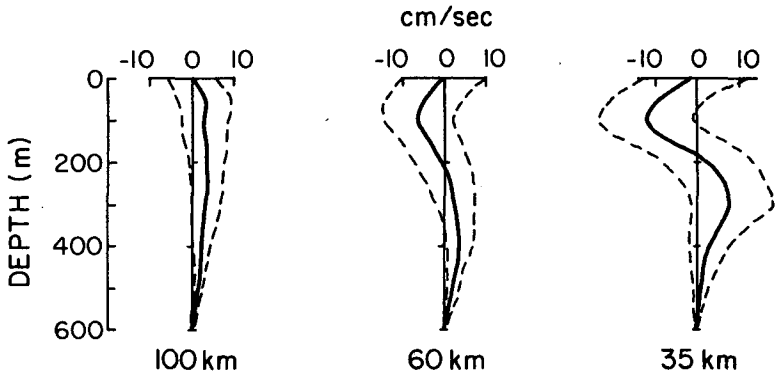

FIG. 9. Vertical profiles of the mean geostrophic velocity relative to 600 db at 35, 60 and 100 km from shore, computed from nine sections between 8 May 1976 and 6 May 1977. Dashed lines show the standard error of the mean. Positive values are northwestward (equatorward) and negative values are southeastward (poleward).

field *et al.*, 1978). These moorings were over the upper slope, between 24 and 28 km from shore, i.e., they were well inshore of the location of the geostrophic velocity profiles shown in Fig. 7. For comparison with the data from the current meter arrays (Fig. 8), the statistics of the geostrophic velocity profiles were recalculated from 18 profiles, omitting the two in August 1976 because of the absence of current meter data for that period. Both the moored current meters and the calculated geostrophic velocities show the presence of a mean poleward (southeastward) undercurrent, whose maximum seems to be at ~100 m. The undercurrent is stronger in the mean geostrophic velocity profile than in the mean profiles obtained from the current meters (Fig. 8). The extra strength could be an artifice of the limited number of geostrophic velocity profiles (18) in the 14-month period, but it may also indicate that the core of the poleward undercurrent lies just seaward of the slope rather than over the upper slope where the current measurements were made. The standard deviation of the low-passed (half-power at 40 h) measured alongshore currents agrees well with the standard deviation of the calculated geostrophic velocities in the upper 200 m, and at 400–500 m; at ~300 m the current meters show less variability than the geostrophic velocity profiles.

Empirical-orthogonal function analysis of the moored current meter records (Brink *et al.*, 1978, 1980) shows that the first two modes account for about 90% of the alongshore variance in each case. The partition of the variance between the first and second modes is surprisingly similar for the various data sets (Fig. 8). The structure of the second modes is also surprisingly similar—in each case the depth of the zero-crossing is between 100 and 200 m. However, the structure of the first mode of the geostrophic velocity profiles is different from the first modes of the direct current observations—the zone of large vertical shear is considerably shallower in the current meter observations over the upper slope than in the geostrophic velocity computed for a location just seaward of the slope. Of course, this difference may be due to the limited sampling, but it may also indicate a real offshore variation in the structure of the vertical modes.

To investigate further the offshore structure of the alongshore velocity and its fluctuations, we also computed geostrophic velocity profiles at 60 and 100 km from shore. Only nine sections had station pairs centered at ~100 km from shore; each pair was separated by 21–32 km. These same nine sections also had station pairs separated by 10–13 km at ~60 km from shore, and station pairs separated by 10–15 km at ~35 km from shore. Profiles of the mean geostrophic velocity computed from these sections (Fig. 9) show the mean surface current is nearly zero at these three locations. The poleward undercurrent has its core at about 100 m, and it is strongest near the continental slope; it is barely discernible 60 km from shore, and is not observed 100 km from shore. Below 300 m the flow is weakly equatorward; near the slope this mean equatorward flow is almost lost in the variability. The complexity of the mean vertical profile seems to decrease with distance from shore—at 100 km, the mean equatorward flow of 3–4 cm s^{-1} is almost independent of depth down to 400 m.

The undercurrent is shallower in these mean profiles (Fig. 9) than in the interpretations of data from the Step-I expedition (Wooster and Gilmartin, 1961; Wyrtki, 1963). Their interpretation was based on water mass analysis as well as on geostrophic computations. Both temperature-salinity characteristics and a chemical signature consisting of low dissolved oxygen, low nitrate and high nitrite concentrations at about 200 m were associated with the Peru-Chile Undercurrent (Wooster, Chow and Barrett, 1965). Our observations suggest that this

chemical signature may instead be a result of essentially no net alongshore flow at this depth.

The standard error of the mean geostrophic velocity (Fig. 9) shows that the variance decreases between 35 and 100 km from shore as expected from Figs. 4 and 5 and the accompanying discussion above. The standard error profiles also show some change in structure with distance from shore, but we attach no significance to this change since nine profiles are not sufficient to define the structure of the fluctuations.

7. Discussion

Sea level variations at the coast off central Peru between April 1976 and May 1977 agree very well with changes in the dynamic height of the sea surface relative to 600 db. The fluctuations are coastally trapped, with an offshore length scale of 30–60 km. The sea level variations are associated with large depth variations of the inshore ends of the 7–11°C isotherms, which lie at depths of 250–500 m, below the strong thermocline. The vertical structure of the associated geostrophic velocity fluctuations shows that the amplitude is constant down to about 300 m, then decreases rapidly down to about 500 m. Brink *et al.* (1978) have shown previously that the sea level fluctuations are not correlated with the local wind, and Smith (1978) has shown that they propagate southward along the Peruvian coast at about 200 km day^{-1}. All of these characteristics are consistent with the idea that the sea level variations are a manifestation of a poleward propagating internal Kelvin wave, but with the interface in the two-layer fluid at about 400 m rather than at the thermocline. The similarity between the offshore length scale of the sea level fluctuations, the width of the continental shelf and slope, and the Rossby radius of deformation suggest that both stratification and topography are important in determining the structure and behavior of the coastally trapped waves in this region. Thus, the observed fluctuations may be modeled most appropriately by a numerical scheme similar to those devised by Wang and Mooers (1976) and Huthnance (1978), which take into account both the actual topography and the mean stratification.

The 14-month sea level record includes some periods of high short-term variability, and some periods with sustained high or low sea level. Sea level is persistently high during April and May 1976, within the period which some authors (e.g., Wyrtki, 1977, 1979) have called the 1976 El Niño. Data from this period show the same general patterns as the data from the remaining JOINT-II period—they do not form separate clusters in the scatter diagrams (Figs. 3 and 6) and they seem to have about the same offshore length scale. Hence, our results may be applicable to the persistent sea level anomalies associated with El Niño as well as to the shorter period fluctuations.

Fluctuations in the geostrophic velocity of the upper layers have an amplitude of about 20–30 cm s^{-1} near the continental slope, decreasing to about 10–20 cm s^{-1} at 100 km from shore. Using a single hydrographic survey without repeated sections to estimate the mean velocity field, therefore, can lead to large errors in the coastal region. Since the amplitude decreases with distance from shore, these errors are probably not too severe at distances more than 150 km from shore. The uncertainty in the coastal region can be reduced considerably if continuous sea level observations are available during such a hydrographic survey: if sea level is essentially constant during the survey, the hydrographic variations are probably spatial in nature. If there are large sea level variations during the survey, some of the hydrographic variability must be temporal; with some repeated hydrographic sections this temporal variability can be estimated, and perhaps separated from the spatial variability. Continuous sea level observations are therefore a very valuable, perhaps essential, element in any program which includes hydrographic surveys of coastal regions.

Acknowledgments. I am grateful to Sr. César Vargas F. and the Dirección de Hidrografía y Navegación de la Marina (Peru) for providing the tide gage data from San Juan. I am also grateful to my colleagues K. H. Brink, D. B. Enfield, R. D. Romea and especially R. L. Smith for many useful discussions related to this paper. W. E. Gilbert, H. Pittock and J. Bottero assisted in the data analysis. This research has been done as part of the Coastal Upwelling Ecosystems Analysis program, supported by the National Science Foundation, Office for the International Decade of Ocean Exploration, under Grant OCE 78-03381.

REFERENCES

Allen, J. S., and R. D. Romea, 1980: On coastal-trapped waves at low latitudes in a stratified ocean. *J. Fluid Mech.*, **98**, 555–585.

Barton, E. D., 1977: JOINT-II-R/V *Thomas G. Thompson* cruise 108 Leg 1, CTD measurements off the coast of Peru near Cabo Nazca, April–May 1976. CUEA Data Rep. 39. University of Washington, Dept. of Oceanography, Ref. M77-76, 140 pp.

Brink, K. H., J. S. Allen and R. L. Smith, 1978: A study of low-frequency fluctuations near the Peru coast. *J. Phys. Oceanogr.*, **8**, 1025–1041.

——, D. Halpern and R. L. Smith, 1980: Circulation in the Peruvian upwelling system near 15°S. *J. Geophys. Res.*, **85**, 4036–4048.

Christensen, N., Jr., and N. Rodríguez S., 1979: A study of sea level variations and currents off Baja California. *J. Phys. Oceanogr.*, **9**, 631–638.

Enfield, D. B., 1980: El Niño: Pacific eastern boundary

response to interannual forcing. *Resource Management and Environmental Uncertainty: Lessons from Coastal Upwelling Fisheries*, M. H. Glantz and J. D. Thomson, Eds., Wiley Interscience (in press).

——, and J. S. Allen, 1980: On the structure and dynamics of monthly mean sea level anomalies along the Pacific coast of North and South America. *J. Phys. Oceanogr.*, **10,** 557–578.

——, R. L. Smith and A. Huyer, 1978: *A Compilation of Observations from Moored Current Meters*, Vol. 13, *Wind, Currents and Temperature over the Continental Shelf and Slope off Peru during JOINT-II*. Oregon State University, School of Oceanography, Data Rep. 70, Ref. 78-4, 343 pp.

Friebertshauser, M. A., D. D. Bishop and L. A. Codispoti, 1977: JOINT-II-R/V *Thomas G. Thompson* cruise 108, Legs II and III, CTD measurements off the coast of Peru near Cabo Nazca, May-June 1976. CUEA Data Report 40, University of Washington, Dept. of Oceanography, Ref. M77-92, 246 pp.

Friederich, G. E., L. A. Codispoti, M. A. Friebertshauser and D. D. Bishop, 1977: JOINT-II, The *Thompson* sections: R/V *T. G. Thompson* cruise 108. CUEA Tech. Rep. 33, University of Washington, Dept. of Oceanography, Ref. M77-91, 45 pp.

Hurlburt, H. E., J. C. Kindle and J. J. O'Brien, 1976: A numerical simulation of the onset of El Niño. *J. Phys. Oceanogr.*, **6,** 621–631.

Huthnance, J. M., 1978: On coastal trapped waves: Analysis and numerical calculation by inverse iteration. *J. Phys. Oceanogr.*, **8,** 74–92.

Huyer, A., and W. E. Gilbert, 1979: Vertical sections and mesoscale maps of temperature, salinity and sigma-*t* off the coast of Peru, July to October 1976 and March to May 1977. Oregon State University, School of Oceanography, Data Rep. 79, Ref. 79-16, 162 pp.

——, W. E. Gilbert, R. Schramm and D. Barstow, 1978a: Temperature and salinity observations off the coast of Peru, R/V *Eastward*, 23 July–16 August 1976. Oregon State University, School of Oceanography, Data Rep. 69, Ref. 78-3, 183 pp.

——, ——, —— and ——, 1978b: CTD observations off the coast of Peru, R/V *Melville*, 4 March–22 May 1977 and R/V *Columbus Iselin*, 5 April–19 May 1977. Oregon State University, School of Oceanography, Data Rep. 71, Ref. 78-18. 409 pp.

Kundu, P. K., J. S. Allen and R. L. Smith, 1975: Modal decomposition of the velocity field near the Oregon coast. *J. Phys. Oceanogr.*, **5,** 683–704.

McCreary, J., 1976: Eastern tropical ocean response to changing wind systems: with application to El Niño. *J. Phys. Oceanogr.*, **6,** 632–645.

Meyers, G., 1979: Annual variation in the slope of the 14°C isotherm along the equator in the Pacific Ocean. *J. Phys. Oceanogr.*, **9,** 885–891.

Pearson, E. S. and H. O. Hartley, Eds., 1970: *Biometrika Tables for Statisticians*, Vol. 1. Cambridge University Press, 270 pp.

Reid, J. L. and A. W. Mantyla, 1976: The effect of the geostrophic flow upon coastal sea elevations in the northern North Pacific Ocean. *J. Geophys. Res.*, **81,** 3100–3110.

Robles P., J. M., and E. D. Barton, 1977: Vertical sections of temperature, salinity and sigma-*t*, JOINT II-R/V *Thomas G. Thompson* cruise 108 leg 1. CUEA Tech. Rep. 35, Centro de Investigación Científica y de Educación, Superior de Ensenada, B.C., México, 38 pp.

Rossby, C.-G., 1938: On the mutual adjustment of pressure and velocity distributions in certain simple current systems, II. *J. Mar. Res.*, **1,** 239–267.

Smith, R. L., 1978: Poleward propagating perturbations in currents and sea levels along the Peru coast. *J. Geophys. Res.*, **83,** 6083–6092.

Tsuchiya, M., 1968: Upper waters of the intertropical Pacific Ocean. *Johns Hopkins Oceanogr. Stud.*, **4,** 50 pp.

——, 1975: Subsurface countercurrents in the eastern equatorial Pacific Ocean. *J. Mar. Res.*, **33**(Suppl.), 145–175.

Wang, D.-P., and C. N. K. Mooers, 1976: Coastal-trapped waves in a continuously stratified ocean. *J. Phys. Oceanog.*, **6,** 853–863.

Wooster, W. S., and M. Gilmartin, 1961: The Peru-Chile Undercurrent. *J. Mar. Res.*, **19,** 97–122.

——, T. J. Chow and I. Barrett, 1965; Nitrite distribution in Peru Current waters. *J. Mar. Res.*, **23,** 210–221.

Wyrtki, K., 1963: The horizontal and vertical field of motion in the Peru Current. *Bull. Scripps Inst. Oceanogr.*, **8,** 313–346.

——, 1975: El Niño—the dynamic response of the equatorial Pacific Ocean to atmospheric forcing. *J. Phys. Oceanogr.*, **5,** 572–584.

——, 1977: Advection in the Peru Current as observed by satellite. *J. Geophys. Res.*, **82,** 3939–3943.

——, 1979: The response of the sea surface topography to the 1976 El Niño. *J. Phys. Oceanogr.*, **9,** 1223–1231.